

Thermoelectric cooling of a finite reservoir coupled to a quantum dot

Stephanie Matern,^{1,2} Saulo V. Moreira,^{3,4} Peter Samuelsson,⁴ and Martin Leijnse²

¹*Pitaevskii BEC Center, CNR-INO and Dipartimento di Fisica, Università di Trento, Trento, Italy*

²*NanoLund and Solid State Physics, Lund University, Box 118, 22100 Lund, Sweden*

³*School of Physics, Trinity College Dublin, Dublin 2, Ireland*

⁴*NanoLund and Mathematical Physics, Lund University, Box 118, 22100 Lund, Sweden*

(Dated: July 11, 2024)

We investigate non-equilibrium transport of charge and heat through an interacting quantum dot coupled to a finite electron reservoir. Both the quantum dot and the finite reservoir are coupled to conventional electric contacts, i.e., infinite electron reservoirs, between which a bias voltage can be applied. We develop a phenomenological description of the system, combining a rate equation for transport through the quantum dot with standard linear response expressions for transport between the finite and infinite reservoirs. The finite reservoir is assumed to be in a quasi-equilibrium state with time-dependent chemical potential and temperature which we solve for self-consistently. We show that the finite reservoir can have a large impact on the stationary state transport properties, including a shift and broadening of the Coulomb diamond edges. We also demonstrate that there is a region around the conductance lines where a heat current flows out of the finite reservoir. Our results reveal the dependence of the temperature that can be reached by this thermoelectric cooling on the system parameters, in particular the coupling between the finite and infinite reservoirs and additional heat currents induced by electron-phonon couplings, and can thus serve as a guide to experiments on quantum dot-enabled thermoelectric cooling of finite electron reservoirs. Finally, we study the full dynamics of the system, with a particular focus on the timescales involved in the thermoelectric cooling.

I. INTRODUCTION

Experimental advances in the fabrication of nanoscale electronic devices have made it possible to employ measurements of non-equilibrium transport to deduce the properties of a (quantum) system. Such devices include a wide range of systems, e.g., molecular junctions, carbon nanotubes, graphene structures and quantum dots (QDs)[1–5]. They are a fundamental building block for applications such as transistors, (thermal) diodes, nanoscale heat engines, and sensors [6–12]. From a theoretical point of view, the description of open quantum systems out of equilibrium remains a challenging task [13]. In non-equilibrium transport scenarios, it is common to assume that the system is in contact with infinite reservoirs at different temperatures and chemical potentials. Although this is a suitable description for a number of experimental situations, accounting for the finite aspect of reservoirs is needed in many nanoscale, non-equilibrium scenarios [14]. Various experiments on, e.g., superconducting [15, 16] or ultracold atom platforms [17] demonstrate intricate control over the non-equilibrium properties of the system, including access to the state of the reservoir [18, 19].

Therefore, finite reservoirs have recently attracted increased attention in theoretical investigations of non-equilibrium phenomena. Efforts to understand how finite reservoirs affect transport properties have involved the development of more appropriate transport models [20, 21], encompassing relaxation processes in QD systems [22] and ultracold atoms [23], many-particle transport [24] and the full system dynamics [25, 26]. Further theoretical works in the literature address temperature

fluctuations in metallic islands [27] and their thermodynamic implications [28]. Considering a finite reservoir as a heat source for an engine, the optimization of such a heat engine’s efficiency has been investigated [29–32].

Particle transport also induces the exchange of energy and heat between different parts of a system. It is natural to consider thermal properties and thermoelectric behavior of finite reservoirs, which are the subject of ongoing interest [33]. Generally, thermoelectric effects describe a system’s or material’s ability to convert a temperature difference to an electric voltage (or vice-versa). A high thermoelectric efficiency results from strong energy asymmetries in electron transport properties [34, 35], which result from sharp resonances in meso- and nanoscale systems [36, 37]. They readily occur in QD devices, promoting QDs to an ideal platform for experimental studies of thermoelectric behavior in quantum devices, see e.g. [12, 38–42]. In particular, an immediate use of thermoelectric properties is Peltier cooling, where a bias voltage can be used to force heat to flow from a cold to a hot reservoir. Such electronic cooling has been realized experimentally using QD systems [43], normal metal-insulator-superconductor junctions [44, 45] and has been investigated in cold atomic gases [46, 47]. In this context, given that any physical device or system being refrigerated is necessarily of a finite size, it is essential to understand transport and thermoelectric behaviors in non-equilibrium settings with finite reservoirs.

In this paper we set out to investigate transport and thermoelectric properties of a system consisting of a finite electron reservoir in contact with a QD. We assume a quasi-equilibrium state of the finite reservoir [22, 24], which can be described by a local equilibrium distribu-

tion. To allow for stationary-state non-equilibrium transport, the system is additionally coupled to two infinite electron reservoirs, see Fig. 1. When there is an applied voltage and/or a temperature difference between the infinite reservoirs, we self-consistently solve for the chemical potential and temperature of the finite reservoir together with the exchanged heat and charge currents, which also means that these quantities become time-dependent. We investigate the transport properties in the stationary state, as well as the full dynamics. We find that the finite reservoir modifies the stationary state properties considerably compared to treating all reservoirs as infinite. Additionally, we discover a parameter regime where heat is carried out of the finite reservoir, resulting in a stationary-state temperature of the finite reservoir *lower* than the temperature of the infinite reservoirs.

The paper is organized as follows. In Section II, the system is introduced, and its non-equilibrium dynamics is modeled using a combination of a rate equation for the QD and a mesoscopic, linear-response approach for the interaction between the finite and infinite reservoirs. In Section III, we solve for the non-equilibrium stationary state and analyse the impact of the finite reservoir on the transport through the QD. The thermoelectric refrigeration of the finite reservoir is discussed in Section IV. Finally, we investigate the system's full dynamics in Section V.

II. MODEL

The system consists of a single level, spin-degenerate QD tunnel-coupled to an infinite reservoir on the right and a finite reservoir on the left, see Fig. 1. The finite reservoir is additionally in contact with a second infinite reservoir to the left. All reservoirs are described by non-interacting electrons. For the finite reservoir we assume that the internal relaxation is fast compared to any other time-scale in the system, such that it is in a quasi-equilibrium state with a well-defined (but time-dependent) chemical potential $\mu_L(t)$ and temperature $T_L(t)$, and is described by the Fermi-Dirac distribution $f(E, \mu_L(t), T_L(t))$ with $f(E, \mu, T) = \{\exp[(E - \mu)/T] + 1\}^{-1}$. Throughout the paper we set Boltzmann's constant $k_B = 1$, the elementary charge $e = 1$ and $\hbar = 1$.

A phenomenological rate equation to describe the transport through the QD system is given by

$$\frac{d}{dt} \begin{pmatrix} p_0 \\ p_1 \end{pmatrix} = \sum_{\alpha} \begin{pmatrix} -\Gamma_{\alpha}^{\text{in}} & \Gamma_{\alpha}^{\text{out}} \\ \Gamma_{\alpha}^{\text{in}} & -\Gamma_{\alpha}^{\text{out}} \end{pmatrix} \begin{pmatrix} p_0 \\ p_1 \end{pmatrix}, \quad (1)$$

where p_0, p_1 denote the probabilities of the QD orbital with energy ϵ being empty or occupied with either a spin-up or a spin-down electron, and $\alpha = L, R$ indexes the left and right reservoirs. At all times $p_0(t) + p_1(t) = 1$ holds. Eq. (1) is valid for a QD system without applied magnetic field, and in the limit of large Coulomb interaction where

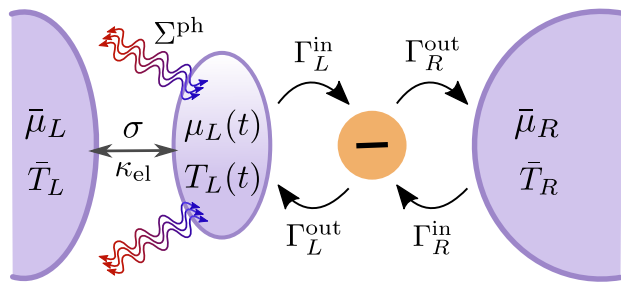


FIG. 1. Sketch of the setup. A QD is coupled to a infinite reservoir on the right. On the left it is coupled to a finite reservoir in a quasi-equilibrium state described by time-dependent $\mu_L(t)$ and $T_L(t)$. $\Gamma_{\alpha}^{\text{in},\text{out}}$ with $\alpha = L, R$ are the rates for tunneling between the QD and the left (finite) and right (infinite) reservoirs. The finite reservoir is in turn in contact with a infinite one. The exchange between them is characterized by the electrical conductivity σ and thermal conductivity κ_{el} . The wavy lines indicate the phonon contribution Σ^{ph} to the heat current due to electron-phonon interaction.

the state with two electrons on the QD can be neglected. The rates for an incoming (or outgoing) electron with respect to the QD from (or to) the left, Γ_L^{in} and Γ_L^{out} , are time-dependent due to the finite nature of the reservoir. They are given by [48]

$$\begin{aligned} \Gamma_L^{\text{in}}(t) &= 2\Gamma_L f(\epsilon, \mu_L(t), T_L(t)), \\ \Gamma_L^{\text{out}}(t) &= \Gamma_L [1 - f(\epsilon, \mu_L(t), T_L(t))], \end{aligned} \quad (2)$$

where Γ_L is the tunneling rate between the QD and finite reservoir. The total rate $\Gamma_L^{\text{in}} \sim 2\Gamma_L$ in Eq. (2) takes into account the spin degeneracy of the state with one electron on the QD. For the exchange with the right reservoir the tunnel rates are time-independent and given by

$$\begin{aligned} \Gamma_R^{\text{in}} &= 2\Gamma_R f(\epsilon, \bar{\mu}_R, \bar{T}_R), \\ \Gamma_R^{\text{out}} &= \Gamma_R [1 - f(\epsilon, \bar{\mu}_R, \bar{T}_R)], \end{aligned} \quad (3)$$

where Γ_R is the tunneling rate between the QD and infinite reservoir. The description of the QD transport with the rate equation (1) is applicable in the weak coupling limit where $\Gamma_{\alpha} \ll T_{\alpha}$. Throughout, we denote the time-independent chemical potential and temperature of the infinite reservoirs with $\bar{\mu}_{\alpha}$ and \bar{T}_{α} with $\alpha = L, R$.

The electron current, $I_{L/R}^{\text{QD}}$, and energy current, $J_{L/R}^{\text{QD}}$, flowing out from the QD to the finite (L) and infinite (R) size reservoirs can be expressed in terms of the QD occupation probabilities and tunnel rates as

$$\begin{aligned} I_{L/R}^{\text{QD}}(t) &= p_1(t)\Gamma_{L/R}^{\text{out}}(t) - p_0(t)\Gamma_{L/R}^{\text{in}}(t), \\ J_{L/R}^{\text{QD}}(t) &= \epsilon I_{L/R}^{\text{QD}}(t). \end{aligned} \quad (4)$$

If $I_L^{\text{QD}} < 0$, the current flows out of the finite reservoir into the QD, while for $I_L^{\text{QD}} > 0$ it flows in the opposite direction.

Assuming the contact between the finite and infinite reservoirs on the left to have energy independent transport properties, the charge and energy currents flowing out of the infinite reservoir are given by [49]

$$\begin{aligned} I_L(t) &= -\sigma\Delta\mu(t), \\ J_L(t) &= -\kappa_{\text{el}}\Delta T(t) + \frac{1}{2}(\mu_L(t) + \bar{\mu}_L)I_L(t). \end{aligned} \quad (5)$$

where we introduced $\Delta\mu(t) = \mu_L(t) - \bar{\mu}_L$ and $\Delta T(t) = T_L(t) - \bar{T}_L$. Here, σ is the electrical conductance and we take the temperature-dependent electronic thermal conductance to be

$$\kappa_{\text{el}}(\tilde{T}(t)) = \frac{\pi^2}{3}\sigma\tilde{T}(t), \quad (6)$$

where $\tilde{T}(t) = (T_L(t) + \bar{T}_L)/2$. In the strict linear response regime, Eq. (6) reduces to the Wiedemann-Franz law [50].

To self-consistently determine the fluctuating $T_L(t)$ and $\mu_L(t)$ of the finite reservoir, we make use of the continuity, or conservation, equations for the charge and energy on the reservoir. The time derivative of the number of electrons of the reservoir, $N_L(t)$, is equal to the sum of the charge currents flowing into the reservoir

$$\dot{N}_L(t) = I_L^{\text{QD}}(t) + I_L(t), \quad (7)$$

where, within our free electron assumption for the finite reservoir, we have

$$\begin{aligned} \dot{N}_L(t) &= \nu_0 \frac{d}{dt} \int dE f[E, \mu_L(t), T_L(t)] \\ &= \nu_0 \dot{\mu}_L(t). \end{aligned} \quad (8)$$

Here, ν_0 is the density of states of the finite reservoir, which we take to be energy independent for simplicity, equal to the quantum capacitance of the reservoir. We note that, for simplicity, we neglect possible geometrical capacitive couplings (e.g., from the other reservoirs) to the excess electrons on the reservoir.

In the same way, the time derivative of the total energy of the finite reservoir is equal to the sum of the energy currents flowing into the reservoir

$$\dot{E}_L(t) = J_L^{\text{QD}}(t) + J_L(t). \quad (9)$$

where

$$\begin{aligned} \dot{E}_L(t) &= \nu_0 \frac{d}{dt} \int dE E f[E, \mu_L(t), T_L(t)] \\ &= \nu_0 \mu_L(t) \dot{\mu}_L + C_{\text{el}}[T_L(t)] \dot{T}_L(t), \end{aligned} \quad (10)$$

where $C_{\text{el}}(T) = \nu_0 \pi^2 T/3$ is the specific heat of a free Fermi gas. Combining Eqs. (7)–(10) we can write

$$\begin{aligned} &C_{\text{el}}[T_L(t)] \dot{T}_L(t) \\ &= J_L^{\text{QD}}(t) + J_L(t) - \mu_L(t) \left[I_L^{\text{QD}}(t) + I_L(t) \right] \\ &\equiv \dot{Q}_L^{\text{QD}}(t) + \dot{Q}_L(t). \end{aligned} \quad (11)$$

Here we introduced the heat currents flowing into the finite reservoir

$$\begin{aligned} \dot{Q}_L^{\text{QD}}(t) &= (\epsilon - \mu_L(t)) I_L^{\text{QD}}(t), \\ \dot{Q}_L(t) &= J_L(t) - \mu_L(t) I_L(t). \end{aligned} \quad (12)$$

This shows that the dynamics of the reservoir temperature $T_L(t)$ is governed by the heat flows into the reservoir, as one would expect. Taken together, Eqs. (1) and (7)–(11) provide a full description of the system dynamics, where the evolution of $\mu_L(t)$ and $T_L(t)$ of the finite reservoir is governed by

$$\begin{aligned} \dot{\mu}_L(t) &= \frac{1}{\nu_0} \left[I_L^{\text{QD}}(t) + I_L(t) \right], \\ \dot{T}_L(t) &= \frac{\dot{Q}_L^{\text{QD}} + \dot{Q}_L(t)}{C_{\text{el}}(T_L(t))}. \end{aligned} \quad (13)$$

A strict linear response approach for a small applied bias reveals two relevant dimensionless parameters governing the stationary transport properties, see Appendix A for details. The first one is $T\sigma/\Gamma_L$. The ratio σ/Γ_L (in units of inverse temperature) characterizes the deviations from a system with only infinite reservoirs in the stationary state, which is apparent from Eqs. (4) and (5). The second parameter, ϵ/T , describes how far from resonance the QD level is.

III. STATIONARY STATE TRANSPORT PROPERTIES

In the following, we determine the transport properties of the set-up shown in Fig. 1 in a non-equilibrium setting. A symmetrically applied bias voltage V_b across the two infinite reservoirs sets their chemical potentials $\bar{\mu}_L = -\bar{\mu}_R = V_b/2$. The energy level ϵ of the QD can be tuned by an additional gate voltage $V_g = -\epsilon$ (for simplicity we set the gate lever arm to unity). Finally, we assume equal temperatures of the infinite reservoirs on the left and right, $\bar{T}_L = \bar{T}_R = T$, as well as equal tunneling rates, $\Gamma_L = \Gamma_R = \Gamma$. We analyse the stationary electron current $I_L^{\text{QD},s} = \lim_{t \rightarrow \infty} I_L^{\text{QD}}(t)$; we use the superscript *s* for the stationary state throughout.

To find the stationary state we solve the coupled equations of motions defined by Eqs. (1) and (7)–(11) for $\dot{\mu}_L = \dot{T}_L = \dot{p}_{0,1} = 0$. The stationary state solution for the probabilities is given by

$$\begin{aligned} p_0^s &= 1 - p_1^s, \\ p_1^s &= \sum_{\alpha=L,R} \frac{\Gamma_{\alpha}^{\text{in},s}}{\Gamma_{\alpha}^{\text{in},s} + \Gamma_{\alpha}^{\text{out},s}}. \end{aligned} \quad (14)$$

A general closed-form expression for the stationary state values for μ_L^s and T_L^s of the finite reservoir is unattainable and we rely on a numerical solution for the transport properties.

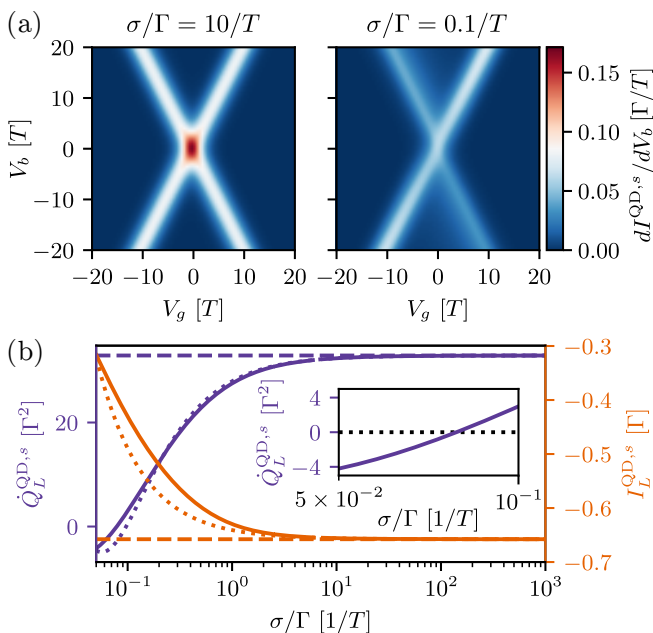


FIG. 2. (a) Stability diagrams showing $dI_L^{\text{QD},s}/dV_b$ as a function of V_b and V_g for two different values of σ/Γ . For $\sigma/\Gamma = 10/T$ the transport looks qualitatively similar to a single level QD coupled to infinite source and drain leads. For $\sigma/\Gamma = 0.1/T$ the visible effects of the finite reservoir include an overall suppression of $I_L^{\text{QD},s}$ and a broadening and shift of one conductance peak. (b) Heat current $\dot{Q}_L^{\text{QD},s}/\Gamma^2$ (purple, left axis) and electron current $I_L^{\text{QD},s}/\Gamma$ (orange, right axis) as a function of σ/Γ at fixed $V_b/T = 10$ and $V_g/T = 0$. The dotted lines show the analytical stationary state solution up to second order in Γ/σ according to Eq. (B6). For large σ/Γ both $\dot{Q}_L^{\text{QD},s}$ and $I_L^{\text{QD},s}$ asymptotically approach the values for the QD coupled to infinite source and drain reservoirs, indicated by the dashed lines. For smaller σ/Γ the stationary state values deviate, and can even lead to $\dot{Q}_L^{\text{QD},s} < 0$, shown in the inset. In all plots $\bar{T}_L = \bar{T}_R = T = 10\Gamma$.

For the stationary current $I_L^{\text{QD},s} = \sigma\Delta\mu$ must hold due to current conservation. Therefore, the magnitude of the current is ultimately limited by σ , if the QD level does not block the transport, i.e., if $\mu_L^s \gtrsim \epsilon \gtrsim \bar{\mu}_R$ for $V_b > 0$. Consequently, we can identify two effects of the finite reservoir on the stationary transport properties compared to coupling of the QD to infinite reservoirs: (i) A modification of the range where electrons can pass through the dot, and (ii) a suppression of the current due to finite σ . There is no strict bound on the temperature T_L^s as the heat current through the system is not conserved. Due to coupling of temperature and chemical potential, there is also no strict bound on μ_L^s . Figure 2(a) shows the differential conductance $dI_L^{\text{QD},s}/dV_b$ for the QD system as a function of V_g and V_b for two different values of σ/Γ . For a single QD coupled to two infinite reservoirs, the stability diagram displays a Coulomb diamond, or a pair of crossing conductance lines for infinite charging energy. Considering now the finite reservoir in Fig. 2(a)

with $\sigma/\Gamma = 10$, changes of μ_L^s in comparison to $\bar{\mu}_L$ are small and the qualitative features of the resulting stability diagram are already similar to the case $\sigma/\Gamma \rightarrow \infty$; this limit corresponds to effectively coupling the QD to two infinite reservoirs.

For smaller values of σ/Γ (focusing on $V_b > 0$), the conductance lines associated with tunneling between the QD and the finite reservoir are broadened and shifted to higher $|V_b|$. To understand this stationary state behavior it is useful to consider the full time dependence. If $\mu_L = \bar{\mu}_L$ at the initial time, electrons tunneling out of the finite reservoir and into the QD will lower μ_L until the current between the infinite and finite reservoirs (given by $\sigma\Delta\mu$) becomes equal to I_L^{QD} . For small σ/Γ , this happens for μ_L close to (or below) ϵ . Thus, in the stationary state μ_L^s is pinned close to ϵ over a range in V_b and the conductance peak shifts and broadens.

The width and position of the conductance peaks associated with tunneling between the QD and right reservoir remain largely unaffected, especially for large V_b, V_g , but their heights are reduced as $I_L^{\text{QD},s}$ is overall suppressed for small σ/Γ . If the QD would also be coupled to a finite reservoir on the right this peak would broaden and shift. For $V_b < 0$ the explanations above hold for reversed inequalities.

We expect our results to remain qualitatively similar for finite values of the Coulomb interaction. The stationary transport properties displayed in Fig. 2(a) would instead show a typical closed Coulomb diamond. However, the conductance lines would be modified in the same way. Similarly, the Zeeman splitting of the QD level due to a magnetic field would not alter the qualitative results.

Further analytical insight can be gained in the regime of large σ/Γ by writing

$$\begin{aligned} \mu_L(t) &= \bar{\mu}_L + \delta\mu_L(t), \\ T_L(t) &= T + \delta T_L(t). \end{aligned} \quad (15)$$

Assuming $\delta\mu_L, \delta T_L$ to be small we expand Eqs. (1) and (13) to first order in the small deviations. This is a good approximation when the finite reservoir is not (significantly) depleted because $\sigma/\Gamma \gg 1$. It does not rely on a small applied bias voltage and is therefore valid beyond a strict linear response theory approach (see Appendix A for the linear-response result). The stationary state solutions for $\delta\mu_L^s$ and δT_L^s are given in Eq. (B1) in Appendix B.

In the limit $\sigma/\Gamma \rightarrow \infty$, $\mu_L^s \rightarrow \bar{\mu}_L$ and $T_L^s \rightarrow T$, and we recover the results of a QD coupled to two infinite reservoirs. This is exemplified by the stationary heat and electron currents shown in Fig. 2(b), including both the full numerical solution (solid lines) and the analytical solution for small $\delta\mu_L^s, \delta T_L^s$ up to second order in Γ/σ (dotted lines).

We find good qualitative agreement of the analytical result with the numerics for the parameters in Fig. 2(b). In general, V_b and ϵ affect the qualitative agreement, and for small V_b the analytics capture the behavior across the

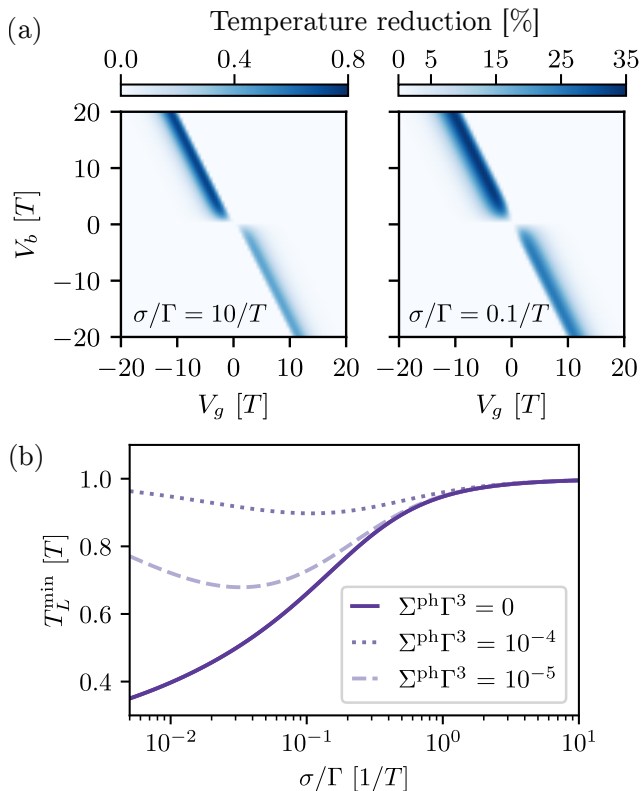


FIG. 3. (a) Temperature reduction for the finite reservoir as a function of V_b and V_g for $\sigma/\Gamma = 10/T$ (left) and $\sigma/\Gamma = 0.1/T$ (right). Plotted is the percentage $|\Delta T^s|/T = |(T_L^s - T)|/T$; regions with heating where $T_L^s > T$ are not shown. (b) T_L^{\min} : T_L^{\min} minimized along cuts of fixed $V_b/T = 10$, plotted as a function of σ/Γ . The dotted and dashed lines indicate T_L^{\min} including the electron-phonon interaction Σ^{ph} in the thermal conductivity. All other parameters are chosen as in Fig. 2.

full range of σ/Γ . The expansion of the analytical results in Eq. (B1) to second order in Γ/σ captures a suppression of the currents $\sim \Gamma/\sigma$ (see also Eq. (B6) in Appendix B) compared to the currents expected for the system if the QD was coupled to infinite reservoirs. However, making σ/Γ smaller than ~ 1 , eventually leads to violating the normalization of the probabilities $p_{0,1}$, which implies a breakdown of the assumption of small deviations.

IV. REFRIGERATION OF THE FINITE RESERVOIR

Under certain conditions, the stationary transport results show a negative heat current $\dot{Q}_L^{\text{QD},s}$ out of the finite reservoir, see Fig. 2(b). Here we investigate under which conditions this leads to refrigeration of the finite reservoir.

The heat current flowing out of the finite reservoir as a result of electrons tunnelling into the QD is given by Eq. (12). For $V_b > 0$, the heat current $\dot{Q}_L^{\text{QD},s}$ is negative

when $\epsilon > \mu_L^s$, because the corresponding electron current $I_L^{\text{QD},s} < 0$. Electrons above the Fermi level are then removed from the finite reservoir and the temperature T_L^s is lowered. In turn, for $V_b < 0$, $I_L^{\text{QD},s} > 0$ and $\dot{Q}_L^{\text{QD},s} < 0$ when $\epsilon < \mu_L^s$, electrons below the Fermi energy μ_L^s are added, again leading to a lower temperature. Achieving cooling also requires the magnitude of the (positive) heat current flowing into the finite reservoir from the infinite reservoir to be smaller than the heat current flowing out to the QD, i.e., $|\dot{Q}_L^s| = |-\kappa_{\text{el}}\Delta T^s + \sigma(\Delta\mu^s)^2/2| < |\dot{Q}_L^{\text{QD},s}|$. If those requirements are fulfilled, a temperature $T_L^s < T$ is induced and the finite reservoir is cooled.

The parameter regime where refrigeration is possible is shown in Fig. 3(a) for two different choices of σ/Γ as a function of V_b and V_g . First, the region in the (V_g, V_b) plane where cooling of the finite reservoir is possible increases for smaller σ/Γ . For $V_b > 0$, this correlates with a larger region where $\epsilon > \mu_L^s$ is fulfilled due to the larger shift of μ_L^s compared to larger σ/Γ . Similarly, for $V_b < 0$ we have instead $\epsilon < \mu_L^s$. Second, the difference between T_L^s and T increases (non-linearly) with decreasing σ/Γ , showing a reduced temperature down to $T_L^s = 0.65T$ for $\sigma/\Gamma = 0.1$. The slight bias asymmetry in the temperature reduction is related to spin degeneracy, which causes an asymmetry between the rates for electrons tunneling in and out of the QD.

A key question for any cooling application is what minimum temperature T_L^{\min} of the finite reservoir can be reached. We determine T_L^{\min} across a line cut at constant V_b (the results only depends very weakly on the choice as long as $V_b \gg T$). The T_L^{\min} that can be reached depending on σ is shown in Fig. 3(b). It keeps decreasing with decreasing σ/Γ , but, as we will see in Section V, the time needed to reach the stationary state increases because the rate of cooling decreases. This also means that the cooling is more sensitive to other sources of heat flows for small σ/Γ .

The phonon contribution to the heat exchange is expected to play an important role in quantum devices [51, 52]. Assuming that the phonon temperature is given by $T_p = T$, the heat current flowing from the finite reservoir into the phonon bath can be included in Eq. (12) through a modified thermal conductivity, where we replace

$$\kappa_{\text{el}} \rightarrow \kappa_{\text{el}} + \Sigma^{\text{ph}}T^4, \quad (16)$$

with the electron-phonon coupling strength Σ^{ph} . For the temperature dependence we choose the typical T^4 for metals [53, 54], however, the exact dependence is not crucial and different exponents are observed experimentally [36]. The phonon contribution becomes more prominent for small σ/Γ , leading to a non-monotonic behaviour of T_L^{\min} as a function of σ/Γ with a clear minimum. The reason is that for small σ/Γ the electron current is lower which corresponds to a lower heat current out of the finite reservoir. This leads to a lower cooling power and therefore a larger impact of the phonons. An additional

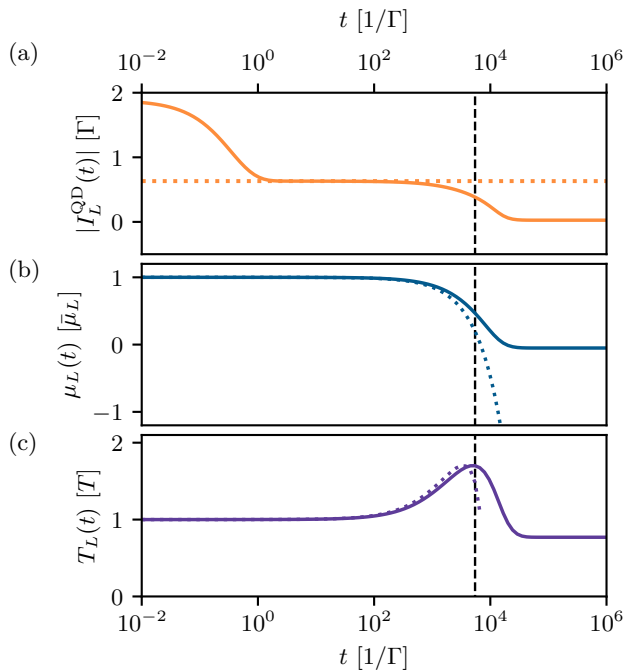


FIG. 4. Full time evolution of (a) $|I_L^{\text{QD}}(t)|$, (b) $\mu_L(t)$ and (c) $T_L(t)$ for the initial condition $\mu_L(0) = \bar{\mu}_L$, $T_L(0) = \bar{T}_L$, $p_0(0) = 1$, $V_b = 10T$, $T = 10\Gamma$, $\epsilon = V_b/4$, $\sigma/\Gamma = 5 \cdot 10^{-3}/T$ and $\nu_0 = 1000/T$. The black dashed line marks the time when $\mu_L(t) = \epsilon$. The dotted line in (a) indicates $I_L^{\text{QD,inf}}$ and the dotted lines in (b) and (c) indicate the evolution according to Eq. (17).

source of heat exchange in this system, with the potential to influence T_L^{min} further, are higher-order tunneling processes [55]. Within the weak coupling regime ($\Gamma \ll T$) studied here, such contributions are small.

V. FULL TIME EVOLUTION

We now investigate the full system dynamics to gain insight into the typical timescales, including the time needed to cool the finite reservoir.

Beyond the stationary state we have access to the full time evolution by numerically integrating the coupled equations of motions for $p_{0,1}(t)$, $\mu_L(t)$ and $T_L(t)$ defined in Eqs. (1) and (13). For further physical insight we focus on a distinct regime where the QD dynamics sets the fastest time scale. We assume $\sigma/\Gamma \ll 1$ and $V_b \gg T$, and we consider an initial state where the finite reservoir is in equilibrium with the left infinite reservoir, and the QD is unoccupied, $p_0(t=0) = 1$. Additionally, we choose $\epsilon/T = V_b/4$, such that the finite reservoir is cooled in the stationary state. The transients for $I_L^{\text{QD}}(t)$, $\mu_L(t)$ and $T_L(t)$ are shown in Fig. 4.

Initially, the fast QD dynamics on the time scale of $\sim 1/\Gamma$ is associated with establishing the QD occupa-

tion p_0^{inf} and current $I_L^{\text{QD,inf}}$ that would be the stationary state values if the QD was coupled to an infinite reservoir. The initial dynamics of $I_L^{\text{QD}}(t)$ is largely independent of $\mu_L(t)$ as long as $\mu_L(t) > \epsilon$ because the Fermi function determining the electron tunneling rate is close to one. In response, $\mu_L(t)$ and $T_L(t)$ adjust for intermediate times $t > 1/\Gamma$ according to

$$\begin{aligned} \dot{\mu}_L(t) &\sim \frac{1}{\nu_0} I_L^{\text{QD,inf}}, \\ \dot{T}_L(t) &\sim \frac{[\epsilon - \mu_L(t)]}{C_{\text{el}} [T_L(t)]} I_L^{\text{QD,inf}}, \end{aligned} \quad (17)$$

which follows from Eq. (13) with $\Delta\mu_L, \Delta T_L \ll 1$ and

$$I_L^{\text{QD,inf}} \sim -2\Gamma p_0^{\text{inf}}. \quad (18)$$

Consequently, the initial downward shift of $\mu_L(t)$ is linear, while $T_L(t)$ first increases as only electrons at energy ϵ can tunnel into the QD, and electrons from below $\mu_L(t)$ are removed from the finite reservoir. As soon as $\mu_L(t) < \epsilon$, \dot{Q}_L^{QD} becomes negative and the finite reservoir eventually starts to cool (although \dot{Q}_L remains positive). Simultaneously, the current decreases since the tunneling rate is sensitive to the tail of the Fermi function. At these later times, the feedback between $\mu_L(t)$, $T_L(t)$ and $p_j(t)$ via the Fermi function $f(\epsilon, \mu_L(t), T_L(t))$ becomes important. We can estimate the longest possible time scale of the system, which is predominately set by σ/ν_0 as the exponential evolution according to $\dot{\mu}_L \sim \sigma\Delta\mu(t)/\nu_0$ and $\dot{T}_L \sim -\sigma(T_L^2(t) - T^2)/C_{\text{el}}(T_L(t))$ from Eq. (13) set in. However, the exact details of how the stationary state is reached depends strongly on the chosen system parameters, as well as the initial condition.

VI. CONCLUSION

In this work, we investigated the non-equilibrium transport properties of a QD coupled to a finite reservoir, as well as two infinite reservoirs. The finite nature of the reservoir leads to (i) a shift of the chemical potential of the finite reservoir which in turn leads to a broadening of one of the conductance peaks in the charge stability diagram; (ii) a suppressed electron current compared to the current that would flow in the case of coupling to infinite reservoirs. Along the conductance peaks we find a region where a temperature T_L^s smaller than the temperature of the infinite reservoirs can be established. Therefore, the electron transport and associated heat flow through a finite reservoir leads to stationary-state refrigeration of that reservoir. This result is immediately relevant for refrigeration applications, as any physical system to be cooled is necessarily finite. The minimum temperature T_L^{min} that can be reached strongly depends on the coupling to the infinite reservoir and is subject to a trade-off. Decreasing σ/Γ results in decreasing T_L^{min} , but also leads to an increasing shift of the chemical potential and

time needed to reach the stationary state. Coupling to phonons strongly impacts T_L^{min} for small σ/Γ , and leads to a minimum of T_L^{min} for finite σ/Γ . Furthermore, we studied the transient dynamics of the system and identified three distinct regimes. An important timescale is set by the ratio of the electrical conductivity with the density of states of the finite reservoir, σ/ν_0 . Therefore, a choice of small σ/Γ for a minimal temperature also leads to slow dynamics towards the stationary state.

Utilizing microscopic approaches [26] for finite reservoirs might provide a promising route to address more complicated quantum systems to further study non-equilibrium transport including fluctuations and noise. But also more fundamental questions such as the modification of the energy distribution [25], especially in quasi-equilibrium or even out-of-equilibrium reservoir states [21] could be addressed.

ACKNOWLEDGMENTS

We would like to thank Viktor Svensson and Konstantin Nestmann for insightful discussions. We acknowledge financial support from the Wallenberg Center for Quantum Technologies (WACQT), the Swedish Research Council (Grant Agreement No. 2020-03412 and No. 2018-03921), and from NanoLund. SM acknowledges financial support from the PNRR-MUR project and PE0000023-NQSTI project, co-funded by the European Union – NextGeneration EU, and from Provincia Autonoma di Trento (PAT). SVM acknowledges funding from the Knut and Alice Wallenberg Foundation (Project No. 2016-0089). This project is co-funded by the European Union (Quantum Flagship project ASPECTS, Grant Agreement No. 101080167). Views and opinions expressed are however those of the authors only and do not necessarily reflect those of the European Union, Research Executive Agency or UKRI. Neither the European Union nor UKRI can be held responsible for them.

Appendix A: Linear response theory for stationary state properties

We consider the stationary electron and energy currents for a small, symmetrically applied bias voltage

ΔV_b across the infinite reservoirs, such that $\bar{\mu}_L = -\bar{\mu}_R = \Delta V_b/2$. There is no temperature gradient across the system, $\bar{T}_L = \bar{T}_R = T$ and we assume equal tunneling rate $\Gamma_L = \Gamma_R = \Gamma$. The chemical potential and temperature of the finite reservoir are

$$\begin{aligned}\mu_L &= \delta\mu_L^s \\ T_L &= T + \delta T_L^s.\end{aligned}\quad (\text{A1})$$

In the strict linear response regime, the quantities $\delta\mu_L^s$ and δT_L^s are proportional to the applied bias ΔV_b . First, the charge and energy currents between the left infinite and finite reservoirs are given by

$$\begin{aligned}I_L &= -\sigma \left(\delta\mu_L^s - \frac{\Delta V_b}{2} \right) \\ J_L &= -\kappa_{\text{el}} \delta T_L^s.\end{aligned}\quad (\text{A2})$$

Second, the particle and energy currents between the QD and the right infinite reservoir are

$$\begin{aligned}I_R^{\text{QD}} &= p_1^s \Gamma_R^{\text{out}} - p_0^s \Gamma_R^{\text{in}}, \\ J_R^{\text{QD}} &= \epsilon I_R^{\text{QD}}.\end{aligned}\quad (\text{A3})$$

In the stationary state, $I_L = I_R^{\text{QD}}$ and $J_L = J_R^{\text{QD}}$ are required. Solving for $\delta\mu_L^s$ and δT_L^s leads to

$$\begin{aligned}\delta\mu_L^s &= \frac{\Delta V_b}{2} \frac{\frac{\sigma}{G} + 3 \left(\frac{\epsilon}{\pi T} \right)^2 - 1}{\frac{\sigma}{G} + 3 \left(\frac{\epsilon}{\pi T} \right)^2 + 1}, \\ \delta T_L^s &= -\Delta V_b \frac{3 \frac{\epsilon}{\pi^2 T}}{\frac{\sigma}{G} + 3 \left(\frac{\epsilon}{\pi T} \right)^2 + 1},\end{aligned}\quad (\text{A4})$$

where we used the Wiedemann-Franz law $\kappa_{\text{el}} = \pi^2 \sigma T/3$ and introduced the conductance

$$G = \frac{\Gamma}{T} \frac{1}{3[1 + \cosh(\epsilon/T)] - \sinh(\epsilon/T)}.\quad (\text{A5})$$

Here, we can identify two independent, dimensionless parameters, ϵ/T and $T\sigma/\Gamma$. The position of the QD level ϵ is crucial as the electron current is exponentially suppressed for $|\epsilon - \bar{\mu}_\alpha| > T$. Additionally, σ/Γ gives a measure of the competing couplings σ (between the infinite and the finite reservoir) and Γ (between finite reservoir and QD).

Appendix B: Large coupling to the infinite reservoir

In the limit of large coupling to the infinite reservoir, $T\sigma/\Gamma \gg 1$, the finite reservoir is barely depleted. We can assume that $\delta\mu_L$ and δT_L in Eq. (15) are small, i.e., $\delta\mu_L \ll \bar{\mu}_L$ and $\delta T_L \ll T$, and we can expand the Fermi functions in the equations of motion (see Eqs. (1) and (13)). The expansion goes beyond a linear response description as it is not limited to small applied bias. To first order in $\delta\mu_L$, δT_L we find closed form expressions in the stationary state,

which are given by

$$\begin{aligned}\delta\mu_L^s &= -\frac{\Gamma}{\sigma} \frac{2\bar{f}_- \bar{T}_L [6\frac{\Gamma}{\sigma} \bar{f}_- (\epsilon - \bar{\mu}_L) - \pi^2 (2 + \bar{f}_+) \bar{T}_L^2]}{(2 + \bar{f}_+) [6\frac{\Gamma}{\sigma} \bar{f}_- (\epsilon - \bar{\mu}_L) - \pi^2 (2 + \bar{f}_+) \bar{T}_L^2] \bar{T}_L - 4\frac{\Gamma}{\sigma} (1 + \bar{f}_R) F_L [\pi^2 \bar{T}_L^2 + 3(\epsilon - \bar{\mu}_L)^2]}, \\ \delta T_L^s &= \frac{\Gamma}{\sigma} \frac{6\bar{f}_- \bar{T}_L^2 [2\frac{\Gamma}{\sigma} \bar{f}_- + (2 + \bar{f}_+) (\epsilon - \bar{\mu}_L)]}{(2 + \bar{f}_+) [6\frac{\Gamma}{\sigma} \bar{f}_- (\epsilon - \bar{\mu}_L) - \pi^2 (2 + \bar{f}_+) \bar{T}_L^2] \bar{T}_L - 4\frac{\Gamma}{\sigma} (1 + \bar{f}_R) F_L [\pi^2 \bar{T}_L^2 + 3(\epsilon - \bar{\mu}_L)^2]}.\end{aligned}\quad (\text{B1})$$

Here, we defined

$$\bar{f}_- = \bar{f}_L - \bar{f}_R, \quad (\text{B2})$$

$$\bar{f}_+ = \bar{f}_L + \bar{f}_R, \quad (\text{B3})$$

$$F_L = \bar{f}_L [1 - \bar{f}_L], \quad (\text{B4})$$

with $\bar{f}_\alpha = f(\epsilon, \bar{\mu}_\alpha, \bar{T}_\alpha)$. The stationary solution for the dot occupation probability according to Eq. (14) within the small-deviations expansion is given by

$$p_1^s = \bar{p}_1^s + \frac{4F_L}{(2 + \bar{f}_+)^2} \left[\frac{\delta\mu_L^s}{\bar{T}_L} + \frac{\epsilon - \bar{\mu}_L}{\bar{T}_L^2} \delta T_L^s \right], \quad (\text{B5})$$

with $\bar{p}_1^s = 2\bar{f}_+ / (2 + \bar{f}_+)$.

The stationary state solution for the small deviations from the infinite reservoir quantities in Eq. (B1) depends explicitly on the ratio Γ/σ , and in the limit of large σ , $\delta\mu_L^s, \delta T_L^s \rightarrow 0$. Expanding Eq. (B1) in the ratio Γ/σ up to second order leads to

$$\begin{aligned}\delta\mu_L^s &\approx -\frac{2\bar{f}_-}{2 + \bar{f}_+} \frac{\Gamma}{\sigma} + \frac{8\bar{f}_- (1 + \bar{f}_R) F_L [\pi^2 \bar{T}_L^2 + 3(\epsilon - \bar{\mu}_L)^2]}{(2 + \bar{f}_+)^3 \pi^2 \bar{T}_L^3} \left(\frac{\Gamma}{\sigma} \right)^2, \\ \delta T_L^s &\approx -\frac{6\bar{f}_- (\epsilon - \bar{\mu}_L)}{(2 + \bar{f}_+) \pi^2 \bar{T}_L} \frac{\Gamma}{\sigma} - \frac{12\bar{f}_- [\bar{f}_- (2 + \bar{f}_+) \bar{T}_L - 2(1 + \bar{f}_R) F_L (\epsilon - \bar{\mu}_L)] [\pi^2 \bar{T}_L^2 + 3(\epsilon - \bar{\mu}_L)^2]}{(2 + \bar{f}_+)^3 \pi^4 \bar{T}_L^4} \left(\frac{\Gamma}{\sigma} \right)^2.\end{aligned}\quad (\text{B6})$$

These solutions are used to calculate the analytical stationary charge and heat current in Fig. 2(b) [dotted lines].

-
- [1] P. Gehring, J. M. Thijssen, and H. S. J. van der Zant, Single-molecule quantum-transport phenomena in break junctions, *Nat. Rev. Phys.* **1**, 381 (2019).
- [2] E. A. Laird, F. Kuemmeth, G. A. Steele, K. Grove-Rasmussen, J. Nygård, K. Flensberg, and L. P. Kouwenhoven, Quantum transport in carbon nanotubes, *Rev. Mod. Phys.* **87**, 703 (2015).
- [3] D. Bischoff, A. Varlet, P. Simonet, M. Eich, H. C. Overweg, T. Ihn, and K. Ensslin, Localized charge carriers in graphene nanodevices, *Applied Physics Reviews* **2**, 031301 (2015).
- [4] W. G. van der Wiel, S. De Franceschi, J. M. Elzerman, T. Fujisawa, S. Tarucha, and L. P. Kouwenhoven, Electron transport through double quantum dots, *Rev. Mod. Phys.* **75**, 1 (2002).
- [5] R. Hanson, L. P. Kouwenhoven, J. R. Petta, S. Tarucha, and L. M. K. Vandersypen, Spins in few-electron quantum dots, *Rev. Mod. Phys.* **79**, 1217 (2007).
- [6] I. Díez-Pérez, J. Hihath, Y. Lee, L. Yu, L. Adamska, M. A. Kozhushner, I. I. Oleynik, and N. Tao, Rectification and stability of a single molecular diode with controlled orientation, *Nat. Chem.* **1**, 635 (2009).
- [7] M. L. Perrin, E. Galan, R. Eelkema, F. Grozema, J. M. Thijssen, and H. S. J. van der Zant, Single-Molecule Resonant Tunneling Diode, *J. Phys. Chem. C* **119**, 5697 (2015).
- [8] G. Benenti, G. Casati, K. Saito, and R. S. Whitney, Fundamental aspects of steady-state conversion of heat to work at the nanoscale, *Physics Reports* **694**, 1 (2017).
- [9] G. Jaliel, R. K. Puddy, R. Sánchez, A. N. Jordan, B. Sothmann, I. Farrer, J. P. Griffiths, D. A. Ritchie, and C. G. Smith, Experimental realization of a quantum dot energy harvester, *Phys. Rev. Lett.* **123**, 117701 (2019).
- [10] F. K. Malik and K. Fobelets, A review of thermal rectification in solid-state devices, *Journal of Semiconductors* **43**, 103101 (2022).
- [11] L. Tesser, B. Bhandari, P. A. Erdman, E. Paladino, R. Fazio, and F. Taddei, Heat rectification through single and coupled quantum dots, *New Journal of Physics* **24**, 035001 (2022).
- [12] M. Josefsson, A. Svilans, A. M. Burke, E. A. Hoffmann, S. Fahlvik, C. Thelander, M. Leijnse, and H. Linke, A quantum-dot heat engine operating close to the thermodynamic efficiency limits, *Nat. Nanotechnol.* **13**, 920 (2018).

- (2018).
- [13] G. T. Landi, D. Poletti, and G. Schaller, Nonequilibrium boundary-driven quantum systems: Models, methods, and properties, *Rev. Mod. Phys.* **94**, 045006 (2022).
- [14] P. Reimann, Foundation of statistical mechanics under experimentally realistic conditions, *Phys. Rev. Lett.* **101**, 190403 (2008).
- [15] A. A. Houck, H. E. Türeci, and J. Koch, On-chip quantum simulation with superconducting circuits, *Nat. Phys.* **8**, 292 (2012).
- [16] S. Schmidt and J. Koch, Circuit QED lattices: Towards quantum simulation with superconducting circuits, *Ann. Phys.* **525**, 395 (2013).
- [17] J.-P. Brantut, J. Meineke, D. Stadler, S. Krinner, and T. Esslinger, Conduction of ultracold fermions through a mesoscopic channel, *Science* **337**, 1069 (2012).
- [18] S. Krinner, T. Esslinger, and J.-P. Brantut, Two-terminal transport measurements with cold atoms, *J. Phys.: Condens. Matter* **29**, 343003 (2017).
- [19] M. Lebrat, P. Grišins, D. Husmann, S. Häusler, L. Corman, T. Giamarchi, J.-P. Brantut, and T. Esslinger, Band and correlated insulators of cold fermions in a mesoscopic lattice, *Phys. Rev. X* **8**, 011053 (2018).
- [20] M. Zwolak, Analytic expressions for the steady-state current with finite extended reservoirs, *The Journal of Chemical Physics* **153**, 224107 (2020).
- [21] A. S. Trushechkin, M. Merkli, J. D. Cresser, and J. Anders, Open quantum system dynamics and the mean force Gibbs state, *AVS Quantum Science* **4**, 012301 (2022).
- [22] G. Schaller, C. Nietner, and T. Brandes, Relaxation dynamics of meso-reservoirs, *New Journal of Physics* **16**, 125011 (2014).
- [23] F. Gallego-Marcos, G. Platero, C. Nietner, G. Schaller, and T. Brandes, Nonequilibrium relaxation transport of ultracold atoms, *Phys. Rev. A* **90**, 033614 (2014).
- [24] G. Amato, H.-P. Breuer, S. Wimberger, A. Rodríguez, and A. Buchleitner, Noninteracting many-particle quantum transport between finite reservoirs, *Phys. Rev. A* **102**, 022207 (2020).
- [25] S. Ajisaka and F. Barra, Nonequilibrium mesoscopic Fermi-reservoir distribution and particle current through a coherent quantum system, *Phys. Rev. B* **87**, 195114 (2013).
- [26] A. Riera-Campenya, A. Sanpera, and P. Strasberg, Quantum systems correlated with a finite bath: Nonequilibrium dynamics and thermodynamics, *PRX Quantum* **2**, 010340 (2021).
- [27] T. L. van den Berg, F. Brange, and P. Samuelsson, Energy and temperature fluctuations in the single electron box, *New Journal of Physics* **17**, 075012 (2015).
- [28] S. V. Moreira, P. Samuelsson, and P. P. Potts, Stochastic thermodynamics of a quantum dot coupled to a finite-size reservoir, *Phys. Rev. Lett.* **131**, 220405 (2023).
- [29] Y. Wang, Optimizing work output for finite-sized heat reservoirs: Beyond linear response, *Phys. Rev. E* **93**, 012120 (2016).
- [30] A. Pozas-Kerstjens, E. G. Brown, and K. V. Hovhannisyan, A quantum otto engine with finite heat baths: energy, correlations, and degradation, *New Journal of Physics* **20**, 043034 (2018).
- [31] P. Strasberg, M. G. Díaz, and A. Riera-Campenya, Clausius inequality for finite baths reveals universal efficiency improvements, *Phys. Rev. E* **104**, L022103 (2021).
- [32] H. Yuan, Y.-H. Ma, and C. P. Sun, Optimizing thermodynamic cycles with two finite-sized reservoirs, *Phys. Rev. E* **105**, L022101 (2022).
- [33] K. Brandner, K. Saito, and U. Seifert, Thermodynamics of micro- and nano-systems driven by periodic temperature variations, *Phys. Rev. X* **5**, 031019 (2015).
- [34] G. D. Mahan and J. O. Sofo, The best thermoelectric., *Proceedings of the National Academy of Sciences* **93**, 7436 (1996).
- [35] T. E. Humphrey and H. Linke, Reversible thermoelectric nanomaterials, *Phys. Rev. Lett.* **94**, 096601 (2005).
- [36] F. Giazotto, T. T. Heikkilä, A. Luukanen, A. M. Savin, and J. P. Pekola, Opportunities for mesoscopics in thermometry and refrigeration: Physics and applications, *Rev. Mod. Phys.* **78**, 217 (2006).
- [37] Y. Dubi and M. Di Ventra, Colloquium: Heat flow and thermoelectricity in atomic and molecular junctions, *Rev. Mod. Phys.* **83**, 131 (2011).
- [38] A. A. M. Staring, L. W. Molenkamp, B. W. Alphenaar, H. van Houten, O. J. A. Buyk, M. A. A. Mabesoone, C. W. J. Beenakker, and C. T. Foxon, Coulomb-blockade oscillations in the thermopower of a quantum dot, *Europhysics Letters* **22**, 57 (1993).
- [39] R. Scheibner, E. G. Novik, T. Borzenko, M. König, D. Reuter, A. D. Wieck, H. Buhmann, and L. W. Molenkamp, Sequential and cotunneling behavior in the temperature-dependent thermopower of few-electron quantum dots, *Phys. Rev. B* **75**, 041301 (2007).
- [40] S. F. Svensson, A. I. Persson, E. A. Hoffmann, N. Nakpathomkun, H. A. Nilsson, H. Q. Xu, L. Samuelson, and H. Linke, Lineshape of the thermopower of quantum dots, *New Journal of Physics* **14**, 033041 (2012).
- [41] A. Svilans, M. Leijnse, and H. Linke, Experiments on the thermoelectric properties of quantum dots, *Comptes Rendus Physique* **17**, 1096 (2016).
- [42] D. Majidi, M. Josefsson, M. Kumar, M. Leijnse, L. Samuelson, H. Courtois, C. B. Winkelmann, and V. F. Maisi, Quantum confinement suppressing electronic heat flow below the Wiedemann–Franz law, *Nano Letters* **22**, 630 (2022).
- [43] J. R. Prance, C. G. Smith, J. P. Griffiths, S. J. Chorley, D. Anderson, G. A. C. Jones, I. Farrer, and D. A. Ritchie, Electronic refrigeration of a two-dimensional electron gas, *Phys. Rev. Lett.* **102**, 146602 (2009).
- [44] J. T. Muhonen, A. O. Niskanen, M. Meschke, Y. A. Pashkin, J. S. Tsai, L. Sainiemi, S. Franssila, and J. P. Pekola, Electronic cooling of a submicron-sized metallic beam, *Applied Physics Letters* **94**, 073101 (2009).
- [45] H. Q. Nguyen, T. Aref, V. J. Kauppila, M. Meschke, C. B. Winkelmann, H. Courtois, and J. P. Pekola, Trapping hot quasi-particles in a high-power superconducting electronic cooler, *New Journal of Physics* **15**, 085013 (2013).
- [46] J.-P. Brantut, C. Grenier, J. Meineke, D. Stadler, S. Krinner, C. Kollath, T. Esslinger, and A. Georges, A thermoelectric heat engine with ultracold atoms, *Science* **342**, 713 (2013).
- [47] C. Grenier, C. Kollath, and A. Georges, Thermoelectric transport and Peltier cooling of cold atomic gases, *C. R. Phys.* **17**, 1161 (2016).
- [48] G.-L. Ingold and Y. V. Nazarov, Charge tunneling rates in ultrasmall junctions, in *Single Charge Tunneling*, edited by H. Grabert and M. H. Devoret (Springer New York, 1992).
- [49] P. Attard, *Non-Equilibrium Thermodynamics and Statis-*

- tical Mechanics* (Oxford University Press, 2012).
- [50] C. Kittel, *Introduction to Solid State Physics*, 8th ed. (John Wiley & Sons, 2005).
- [51] D. G. Cahill, P. V. Braun, G. Chen, D. R. Clarke, S. Fan, K. E. Goodson, P. Keblinski, W. P. King, G. D. Mahan, A. Majumdar, H. J. Maris, S. R. Phillpot, E. Pop, and L. Shi, Nanoscale thermal transport. II. 2003–2012, *Applied Physics Reviews* **1**, 011305 (2014).
- [52] X. Qian, J. Zhou, and G. Chen, Phonon-engineered extreme thermal conductivity materials, *Nat. Mater.* **20**, 1188 (2021).
- [53] J. P. Pekola and B. Karimi, Quantum Noise of Electron–Phonon Heat Current, *J. Low Temp. Phys.* **191**, 373 (2018).
- [54] F. Brange, P. Samuelsson, B. Karimi, and J. P. Pekola, Nanoscale quantum calorimetry with electronic temperature fluctuations, *Phys. Rev. B* **98**, 205414 (2018).
- [55] M. Turek and K. A. Matveev, Cotunneling thermopower of single electron transistors, *Phys. Rev. B* **65**, 115332 (2002).